Numerical Simulation of Film Coating Process in a Novel Rotating Fluidized Bed

Hideya NAKAMURA, Tomohiro IWASAKI, and Satoru WATANO*

Department of Chemical Engineering, Osaka Prefecture University; 1–1 Gakuen-cho, Naka-ku, Sakai, Osaka 599–8531, Japan. Received January 10, 2006; accepted March 9, 2006; published online March 15, 2006

In this study, numerical simulation of film coating process in a novel rotating fluidized bed (RFB) was conducted by using a Discrete Element Method (DEM)–Computational Fluid Dynamics (CFD) coupling model. Particle movements and fluid motions in a centrifugal force field were simulated at three-dimensional cylindrical coordinate, and this model was applied to film coating process. Film coating process in a RFB was numerically analyzed by using a simplified assumption that a particle was coated only when a particle existed within a spray zone. The experiments were also conducted and uniformity of sprayed material was evaluated by investigating color difference of the coated particles. As a result of the numerical simulation, three-dimensional bubble movements and particle circulation could be well simulated. In addition, mass of the sprayed material on a single particle in a RFB could be visualized by using our proposed model. The relationship between distribution of the sprayed material and the coating time was also analyzed. Calculated mass distributions of the sprayed material could be expressed by a normal distribution function, showing qualitative good agreement with the previous studies. Effect of the operating parameters, such as gas velocity and centrifugal acceleration, on the uniformity of the sprayed material was also investigated by both numerical and experimental approaches. Comparison of the coating process in a RFB with that in a conventional fluidized bed was also conducted by the numerical simulation. The result showed that uniformity of the sprayed material was greatly improved in a RFB due to the much smaller circulation time.

Key words rotating fluidized bed; film coating process; numerical simulation; discrete element method; computational fluid dynamics

Particle coating process has been widely employed in many industries, such as food, agriculture, cosmetic and pharmaceutical industries, in order to produce functional materials. Among many types of particle coating system, fluidized bed is one of the most promising techniques because of its advantages of high heat transfer, temperature homogeneity, high mixing performance, flowability of particulate materials, and availability of multilayer coating capability.

Recently, fine particles, having size range between several micrometers and nanometers, have become major interest in many industries. In the pharmaceutical industry, fine particles have been expected for novel drug delivery systems, such as asthma therapy by inhalation or cancer therapy by transcatheter arterial embolization. However, according to the Geldart's classification,[1] it is very difficult to fluidize fine particles in group C having diameters less than 20 μm, because of the strong cohesive forces between fine particles. Therefore, a reliable technique for fluidization of fine particles and giving tailored functions to them is strongly required. So far, we have developed a novel rotating fluidized bed (RFB) in order to fluidize fine powders.[2—4] Since the RFB can impart high centrifugal force and drug force to particles, which are larger than the cohesive forces, the RFB enables fine particles to fluidize uniformly. We have already reported that wet granulation[2] and film coating[3,4] of fine particles (group C in the Geldart's classification) could be smoothly conducted in a RFB, in which any conventional fluidization techniques have been impossible to do. However, the particle fluidization behaviors in a RFB are very complicated, and mechanisms of film coating process have not been well studied yet. From the viewpoint of "Quality by Design (QBD)," it is very important to propose a model for film coating process and analyze the relationship between the operating conditions and quality of products, such as uniformity of coated material, in a RFB.

There are some studies on numerical simulation of film coating process in a fluidized bed, such as a population balance model in a conventional fluidized bed[5] and Monte Carlo simulation in a tumbling fluidized bed.[6] However, these models are very complicated and calculation results strongly depend on the model parameters. By contrast, a DEM–CFD coupling model[7] is one of the most useful numerical models of fluidized bed. In this model, individual particle motion and fluid motion are calculated by a discrete element method (DEM) and a numerical method of computational fluid dynamics (CFD). In the DEM simulation, individual particle motion can be calculated based on 'first principle'; integrating the Newton's second law for individual particle, allowing for external forces, such as contact forces, drag force and *etc.*, acting on each particle. Therefore, it is expected that film coating process can be well simulated by using a DEM–CFD coupling model. However, there is no report on numerical simulation of film coating process in a fluidized bed, as well as in a RFB.

In this study, a three-dimensional particle fluidization model in a RFB was proposed by a DEM–CFD coupling model. This model was then applied to film coating process in a RFB. Visualization of fluidization behaviors and distribution of sprayed material on a single particle was conducted by our proposed model. The relationships between the operating parameters, such as coating time, gas velocity and centrifugal acceleration, and sprayed material distributions were also analyzed by both numerical and experimental results. In addition, comparison of coating process in a RFB with that in a conventional fluidized bed was also conducted by the numerical simulation.

* To whom correspondence should be addressed. e-mail: watano@chemeng.osakafu-u.ac.jp

Numerical Model

Motion of Fluid The calculation of fluid motion is based on the locally averaged equation of continuity and equation of motion.[8] Here, the fluid was assumed as incompressible and inviscid due to the strong interaction between particle and fluid, and three-dimensional cylindrical coordinate (r, θ, z) was employed. The basic equations are given as follows:

Equation of continuity

$$\frac{\partial}{\partial t}\varepsilon+\frac{1}{r}\frac{\partial}{\partial r}(\varepsilon u_r r)+\frac{1}{r}\frac{\partial}{\partial \theta}(\varepsilon u_\theta)\frac{\partial}{\partial z}(\varepsilon u_z)=0 \tag{1}$$

Equations of motion

r-direction

$$\frac{\partial}{\partial t}(\varepsilon u_r)+\frac{1}{r}\frac{\partial}{\partial r}(\varepsilon u_r u_r r)+\frac{1}{r}\frac{\partial}{\partial \theta}(\varepsilon u_r u_\theta)-\frac{\varepsilon u_\theta u_\theta}{r}+\frac{\partial}{\partial z}(\varepsilon u_r u_z) =-\frac{\varepsilon}{\rho_f}\frac{\partial P}{\partial r}-\frac{f_{ir}}{\rho_f} \tag{2}$$

θ-direction

$$\frac{\partial}{\partial t}(\varepsilon u_\theta)+\frac{\partial}{\partial r}(\varepsilon u_r u_\theta)+\frac{1}{r}\frac{\partial}{\partial \theta}(\varepsilon u_\theta u_\theta)+\frac{2}{r}\varepsilon u_r u_\theta+\frac{\partial}{\partial z}(\varepsilon u_r u_z) =-\frac{\varepsilon}{\rho_f}\frac{1}{r}\frac{\partial P}{\partial \theta}-\frac{f_{i\theta}}{\rho_f} \tag{3}$$

z-direction

$$\frac{\partial}{\partial t}(\varepsilon u_z)+\frac{1}{r}\frac{\partial}{\partial r}(\varepsilon u_r u_z r)+\frac{1}{r}\frac{\partial}{\partial \theta}(\varepsilon u_\theta u_z)+\frac{\partial}{\partial z}(\varepsilon u_z u_z) =-\frac{\varepsilon}{\rho_f}\frac{\partial P}{\partial z}-\frac{f_{iz}}{\rho_f} \tag{4}$$

where, ε, u, P are the voidage, the gas velocity, the gas pressure, and ρ_f and f_i are the gas density and the volumetric interaction forces between particle and fluid. The f_i in Eqs. (2)—(4) are also given by the following equations[9] based on the Ergun's equation[10] for the dense phase ($\varepsilon \leqq 0.8$) and Wen and Yu's equation[11] for the dilute phase ($\varepsilon > 0.8$):

$\varepsilon \leq 0.8$;

$$\boldsymbol{f}_i=150\frac{(1-\varepsilon)^2}{\varepsilon}\frac{\mu_f}{d_p^2}(\boldsymbol{u}-\bar{\boldsymbol{V}})+1.75(1-\varepsilon)\frac{\rho_f|\boldsymbol{u}-\bar{\boldsymbol{V}}|}{d_p}(\boldsymbol{u}-\bar{\boldsymbol{V}}) \tag{5}$$

$\varepsilon > 0.8$;

$$\boldsymbol{f}_i=\frac{\varepsilon}{\Delta V}\sum_{j=1}^{n_c}\left[\frac{\pi}{8}C_D\rho_f\varepsilon^{-2.65}|\boldsymbol{u}-\boldsymbol{V}_j|(\boldsymbol{u}-\boldsymbol{V}_j)d_p^2\right] \tag{6}$$

$$C_D=\begin{cases}24(1+0.15Re^{0.687})/Re & (Re\leq 1000)\\ 0.44 & (Re>1000)\end{cases}$$

$$Re=\frac{\rho_f\varepsilon d_p|\boldsymbol{u}-\bar{\boldsymbol{V}}|}{\mu_f}$$

where, $\boldsymbol{u}$ and $\boldsymbol{V}$ are the gas velocity vector and individual particle velocity vector. $\bar{\boldsymbol{V}}$ is the average particle velocity vector in a fluid cell. μ_f, d_p, ΔV, and n_c are the gas viscosity, the particle diameter, the volume of a fluid cell, and the number of particle in a fluid cell, respectively. C_D is the drag coefficient depending on particle Reynolds number.

The fluid motion was calculated by numerically solving Eqs. (1)—(4). In the present model, SIMPLE method[12] was used as the numerical calculation scheme.

Motion of Particle For the modeling of particle motion, a three-dimensional discrete element method (DEM) was used. The DEM calculates the motion of each particle by integrating the Newton's second law for individual particle step by step, allowing for the external forces acting on a single particle. Equations of translational and rotational motions for individual particle are as follows:

$$m\frac{d^2\boldsymbol{X}}{dt^2}=\boldsymbol{F}_c+\boldsymbol{F}_d+\boldsymbol{F}_{cen}+\boldsymbol{F}_{cori}+m\boldsymbol{g} \tag{7}$$

$$\frac{d\boldsymbol{\omega}_p}{dt}=\frac{\boldsymbol{T}}{I} \tag{8}$$

where, $\boldsymbol{X}$, m, t are the position vector, mass of a particle and time, and $\boldsymbol{F}_c$, $\boldsymbol{F}_d$, $\boldsymbol{F}_{cen}$ and $\boldsymbol{F}_{cori}$ indicate contact, drag, centrifugal and coriolis forces, respectively. Also, $\boldsymbol{g}$, $\boldsymbol{\omega}_p$, $\boldsymbol{T}$ and I show gravitational acceleration, angular velocity, moment by contact, and inertia moment.

For estimation of particle contact force, a contact model shown in Fig. 1 proposed by Cundall and Strack[13] was used. This model estimates the contact forces by using mechanical elements such as a spring, dash pot and friction slider. To simplify the model, particles and wall were assumed to be uniform elastic body. The contact forces of normal and tangential direction, which are described as $\boldsymbol{F}_{cn}$ and $\boldsymbol{F}_{ct}$, are given as follows:

$$\boldsymbol{F}_{cn}=(-k\delta_n-\eta\boldsymbol{V}_r\cdot\boldsymbol{n})\boldsymbol{n} \tag{9}$$

$$\boldsymbol{F}_{ct}=(-k\cdot\boldsymbol{\delta}_t-\eta\boldsymbol{V}_{rt}) \quad (\text{if } |\boldsymbol{F}_{ct}|\leq\mu|\boldsymbol{F}_{cn}|) \tag{10}$$

$$\boldsymbol{F}_{ct}=-\mu|\boldsymbol{F}_{cn}|\frac{\boldsymbol{V}_{rt}}{|\boldsymbol{V}_{rt}|} \quad \left(\text{if } |\boldsymbol{F}_{ct}|>\mu|\boldsymbol{F}_{cn}|\right) \tag{11}$$

where, δ, k, η and μ are displacement between contact particles, stiffness of spring, damping coefficient and friction coefficient, and $\boldsymbol{V}_r$ shows relative particle velocity between contact particles, respectively. The damping coefficient η is calculated by the following equation[7]:

$$\eta=-\frac{2\ln e}{\sqrt{\pi^2+\ln e}}\sqrt{mk} \tag{12}$$

where e shows the coefficient of restitution.

The drag force $\boldsymbol{F}_d$ is given as the reaction force of Eqs. 5 and 6 as following equations[9]:

$\varepsilon \leq 0.8$;

$$\boldsymbol{F}_d=\frac{\boldsymbol{f}_i}{\varepsilon n_c}\Delta V \tag{13}$$

$\varepsilon > 0.8$;

$$\boldsymbol{F}_d=\frac{\pi}{8}C_D\rho_f\varepsilon^{-2.65}|\boldsymbol{u}-\boldsymbol{V}|(\boldsymbol{u}-\boldsymbol{V})d_p^2 \tag{14}$$

The centrifugal ($\boldsymbol{F}_{cen}$) and coriolis ($\boldsymbol{F}_{cori}$) forces are calculated by the following equations:

$$\boldsymbol{F}_{cen}=\frac{mV_\theta^2}{r} \tag{15}$$

$$\boldsymbol{F}_{cori}=-2m\frac{V_r V_\theta}{r} \tag{16}$$

The motion of all particles is calculated by numerically integrating the Eqs. 7 and 8 with respect to time from t to $t+\Delta t$.

In the DEM simulation, it is very important to define the proper time step of calculation (Δt). Assuming the linear spring model, specific vibration period T_d in a mass-spring system is calculated by Eq. 17.

$$T_d = 2\pi\sqrt{\frac{m}{k}} \tag{17}$$

It has been reported that the time step smaller than 1/10 of the specific vibration period T_d is required for the stable calculation.[7] In this study, the calculation of fluid and particle motions were conducted under the condition that the time step (Δt) was 1.5×10^{-5} s.

In the present model, the particle fluidization behaviors in a RFB were numerically analyzed by simultaneously solving the particle and fluid motions for each time step. This numerical calculation, which is a combination of discrete element method (DEM) and computational fluid dynamics (CFD), is called as a DEM–CFD coupling model.[7]

Calculation Conditions Figure 1 also shows fluid cell configuration in the present model. Table 1 also shows computational domain and size for the fluid cell. In the present model, the fluid cell was defined as having variable sizes in the r-direction, while as having constant division numbers in the θ and z-direction. It has been reported that the fluid cell should contain more than 10 particles to avoid computational error that would result from improper local average of fluid motion.[14] Therefore, for the stable calculation, cell sizes were defined as sufficient size by using proper valuable cell sizes in the r-direction. At the outside boundary (air distributor), it was assumed that the gas flows inward uniformly from outside. The fluid velocity at the outside boundary was assumed to be the superficial gas velocity u_0. The outside boundary wall was also assumed to be a slip wall, and had a certain rotational velocity.

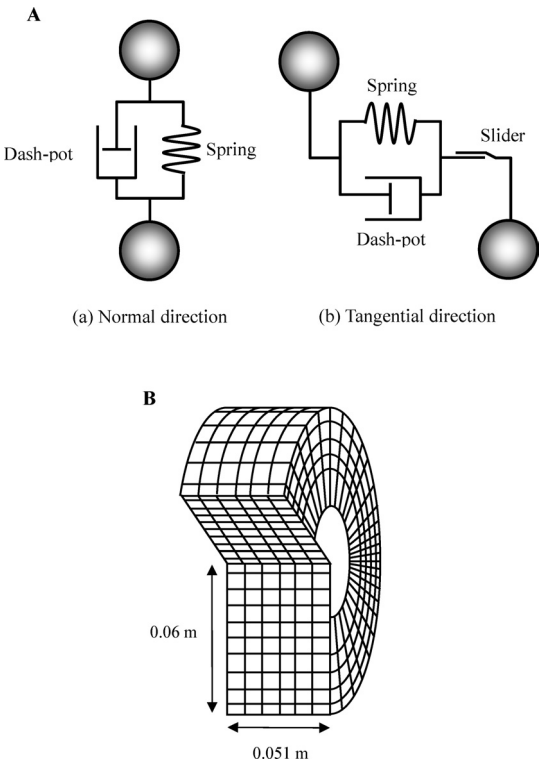

Fig. 1. Models of Contact Force (A) and Fluid Cell Configuration (B)

Table 1. Computational Domain and Size for Fluid Cell

	r-direction	θ-direction	z-direction
Computational domain	6.0×10^{-2} [m]	2π [rad]	0.051 [m]
Cell size	3.0—6.0×10^{-3} [m]	$2\pi/30$ [rad]	0.0051 [m]
Number of grid points	12	30	10

Before starting particle fluidization, initial condition of particle configuration was pre-calculated as follows. First of all, all particles were orderly arranged (Fig. 2a). All particles were then fell down by gravity force with rotation of the boundary wall having a certain rotational speed. When particles motion became steady state, pre-calculations were completed and these conditions were used as the initial conditions of particle configurations (Fig. 2b). Bed height was almost 1.2 cm, and required pre-calculation time of particle motion was 2.0 s.

Table 2 shows calculation conditions in this study. For both simulation and experiment, spherical crystalline cellulose granules were used. In the simulation, it is assumed that the particles were cohesionless and mono-disperse. The diameter of model particles was set at 2.0 mm, which is so much larger than fine particle diameter, for reducing calculation time. This diameter of model particle seems to be insufficient for modeling of fine particle handling process as mentioned previously. Theoretically, if the vessel rotates at a high enough speed and the airflow increases correspondingly to keep a uniform fluidization, the interparticle forces between fine particles can be neglected as compared to the high centrifugal and drag forces in a RFB.[15] Therefore, an analysis of a handling process of fine particle can be sufficiently conducted, even if the diameter of model particle was set at 2.0 mm.

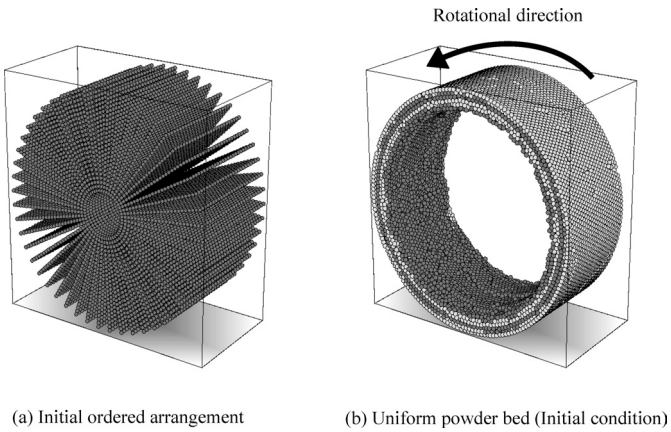

Fig. 2. Initial Condition of Particle Configuration

Table 2. Calculation Conditions

Vessel diameter	0.12	[m]
Vessel depth	0.051	[m]
Number of particle	30000	[—]
Particle diameter	2.0×10^{-3}	[m]
Stiffness of spring	5000	[N m^{-1}]
Restitution coefficient	0.90	[—]
Friction factor (particle–particle)	0.32	[—]
Friction factor (particle–rotating vessel)	0.34	[—]
Friction factor (particle–front and backside wall)	0.23	[—]
Particle density	1373	[kg m^{-3}]
Air density	1.205	[kg m^{-3}]
Air viscosity	1.8×10^{-5}	[Pa s]
Time step	1.5×10^{-5}	[s]

It is also important to define proper model parameters in DEM simulation. In this study, stiffness of spring was determined from theoretical prediction. Mikami[14] reported that stiffness of spring could be arbitrarily chosen, if maximum overlap distance at collision is sufficiently small. He also reported that when dimensionless maximum overlap distance, δ/d_p, was less than 10%, calculation was sufficiently conducted in his system. The dimensionless maximum overlap distance, δ/d_p, can be calculated by the following equation[14]:

$$\delta/d_p=(\pi d_p\rho_p/6k)^{0.5}|V_r| \tag{18}$$

In this study, stiffness of spring was determined in the range of less than 5% of maximum overlap distance δ/d_p. Here, relative velocity ($|V_r|$) before collision was assumed to be the vessel tangential rotational speed at 40 G (4.85 m/s). From these considerations, stiffness of spring was set at 5000 N/m.

Friction factors were determined experimentally by using a friction tester shown in Fig. 3. The friction tester could measure maximum static friction force between powder beds, or powder bed and vessel wall. In this study, the simulated friction force at collision was assumed to be equivalent to static friction force as mentioned above.

Modeling of Film Coating Process In a film coating process, particle coating is conducted through the cycle of following processes: (1) Contact and adhesion of sprayed mist onto core particle→(2) Drying and formation of film on a particle surface→(3) Re-contact and adhesion of sprayed mist onto core particle (Fig. 4). Therefore, for modeling of film coating process, it is very important to analyze the residence time of a particle in the spray zone and the number of passes of a particle thorough the spray zone.

In this study, film coating process in a RFB was numerically analyzed by the DEM–CFD coupling model by using a simplified model, which assumed that coating was conducted only when a particle existed within the stationary conical spray zone as shown in Fig. 4. Here, tip of conical was located on the central position in a cylindrical vessel, conical height was the same as inner radius of particle bed, and spray zone was set at top of the vessel. In the numerical simulation, mass of the sprayed material (C_m) on a single particle was calculated by dividing the residence time of a particle in the spray zone by calculation time step for DEM simulation. Variation coefficient of calculated mass of the sprayed material ($Cv_{calc.}$) was also calculated by the following equation:

$$Cv_{calc.}=\frac{\sigma}{\overline{C}_m}=\frac{1}{\overline{C}_m}\sqrt{\frac{1}{N}\sum_{i=1}^{N}(C_{mi}-\overline{C}_m)^2} \tag{19}$$

where, σ, $\overline{C}_m$, and N show standard deviation of mass of the sprayed material, mean mass of the sprayed material and total number of particles, respectively.

The assumptions in modeling of coating process are as follows:

1. Conditions of spray zone were not affected by fluidization gas.
2. Particle motion and fluidization gas motion were not affected by sprayed air.
3. Concentration of sprayed mist was uniform in the conical spray zone.
4. Agglomeration by liquid bridge was not occurred.

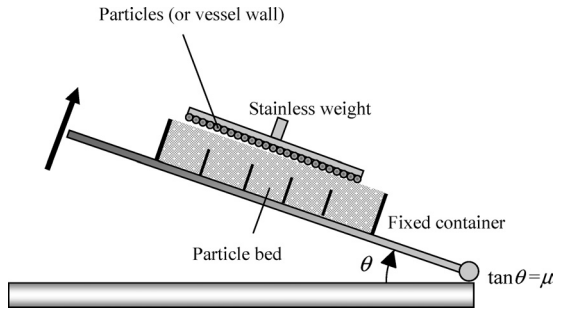

Fig. 3. Schematic Diagram of Friction Tester for Determination of Friction Factor

Experimental

The experiments were also conducted. Figure 5 shows a schematic diagram of a rotating fluidized bed coater.[2–4] A rotating fluidized bed coater consists of a plenum chamber and a porous cylindrical air distributor (ID 0.4 m×D 0.1 m) made of stainless sintered mesh with 20 mm openings. The horizontal cylinder (air distributor) rotates around its axis of symmetry inside the plenum chamber. The front covers of the chamber and rotating air distributor are both made of transparent acrylic plastic that allows observation of the particle fluidization behavior. There is a stationary concentric cylindrical bag filter inside the air distributor to retain elutriated particles.

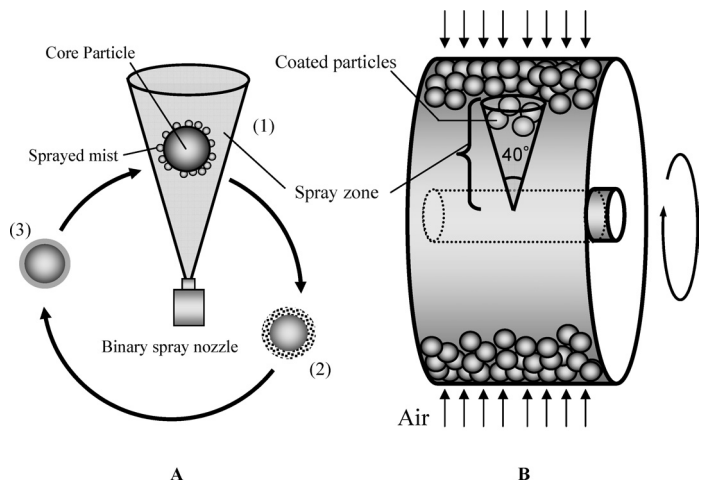

Fig. 4. Mechanism of Film Coating Process (A) and Conical Spray Zone (B)

A(1), (2), and (3) indicate following that; (1) contact and adhesion of sprayed mist onto core particle; (2) drying and formation of film on a particle surface; and (3) re-contact and adhesion of sprayed mist onto core particle, respectively.

Air flows inward through the air distributor, and particles are balanced by the drag and centrifugal forces, leading to achieve fluidization condition. A binary spray nozzle mounted on the bag filter, and coating material was sprayed onto fluidized particle bed. In this study, 5.0% aqueous solution of pigment food blue No. 1 (Izumiya Shikiso) was used as the model coating material. Crystalline cellulose particle (Celphere CP-100, Asahikasei Co., Ltd.) with a mass median diameter of 120 μm was used as the model core particle. Table 3 lists the operating conditions of the experiments.

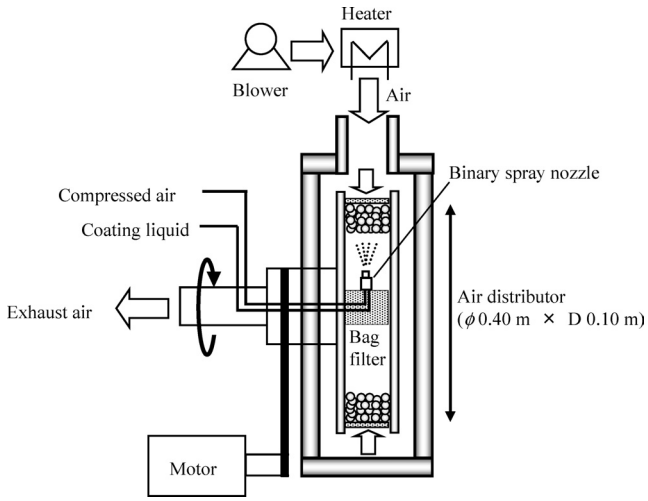

Fig. 5. Experimental Apparatus: Novel Rotating Fluidized Bed Coater

Table 3. Experimental Conditions

Fluidization gas temperature	303	[K]
Spray air pressure	0.30	[MPa]
Liquid feeding rate	7.0	[g min^{-1}]
Charged mass of core particles	800	[g]

Evaluation of the uniformity of sprayed material was conducted as follows; Coated particles were divided into 25 sample spots, and the colorfulness b for each sample spot was measured by using a chroma meter (CL-100, MINOLTA Co., Ltd.). Variation coefficient of the colorfulness ($Cv_{exp.}$) was then calculated by the following equation:

$$Cv_{exp.} = \frac{\sigma}{\bar{b}} = \frac{1}{\bar{b}} \sqrt{\frac{1}{n_s - 1} \sum_{i=1}^{n_s} (b_i - \bar{b})^2} \tag{20}$$

where, σ, $\bar{b}$, and n_s indicate standard deviation of colorfulness b, mean colorfulness and total number of sample spots, respectively.

Results and Discussion

Visualization of Particle Fluidization Behaviors and the Sprayed Material Distributions Figure 6(a) shows the calculated three-dimensional particle fluidization behavior in a RFB. Figure 6(b) also illustrates z-directional cross-section of particle fluidization behavior. The periodic three-dimensional fluidization behaviors, such as the bubble formation, coalescence, eruption and particle circulation with rotational motion, could be well simulated by our proposed model.

Figure 7 shows the mass of the sprayed material on individual particle at different coating times. With an increase in a coating time, the mass of sprayed material increased, *i.e.*, particle's color became closer to red. Therefore, distributions

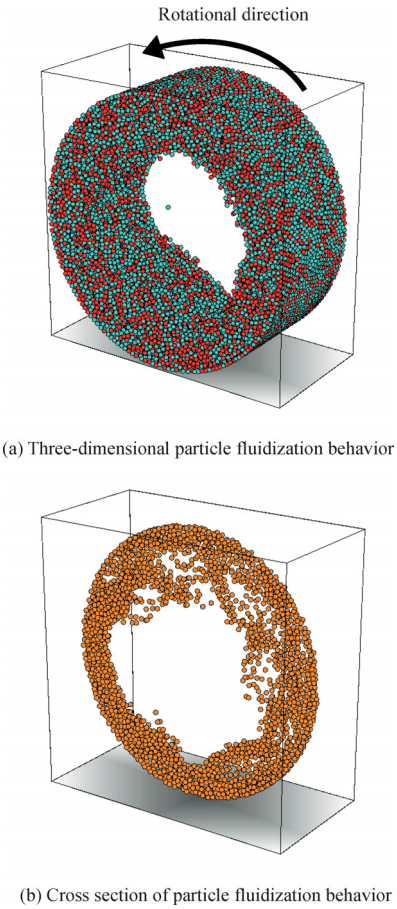

(a) Three-dimensional particle fluidization behavior

(b) Cross section of particle fluidization behavior

Fig. 6. Calculated Three-Dimensional Particle Fluidization Behavior in a RFB (10 G, u_0=1.8u_{mf})

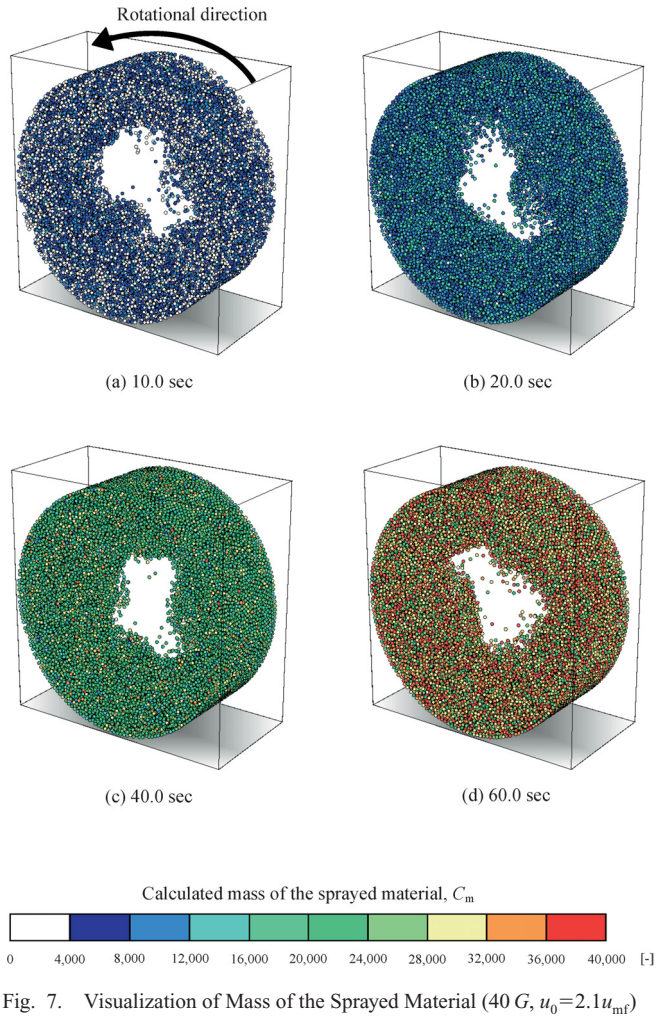

Fig. 7. Visualization of Mass of the Sprayed Material (40 G, u_0=2.1u_{mf})

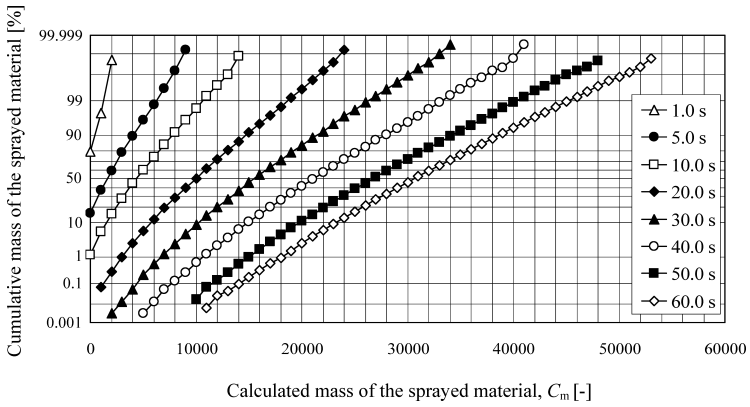

Fig. 8. Calculated Mass Distribution of the Sprayed Material (40 G, u_0=2.1u_{mf})
The results were plotted on a normal probability graph.

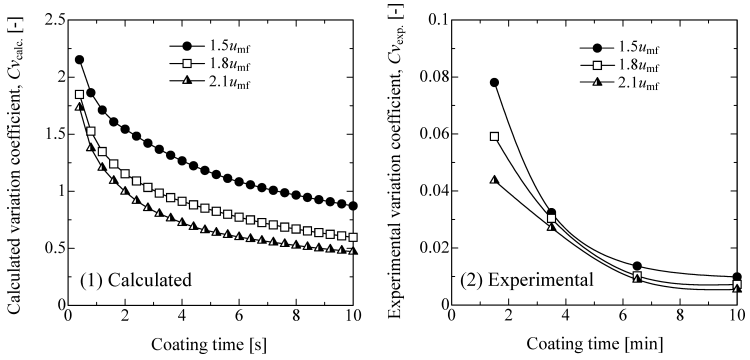

Fig. 9. Temporal Change in the Variation Coefficient of Mass Distribution at Different Gas Velocities
(1) and (2) show the calculated and experimental results, respectively. Centrifugal acceleration was set at 10 G. Each solid line shows spline approximation curve.

of the sprayed material on individual particle could be well visualized by using our proposed model. It is also considered that DEM simulation is the only method for visualization of the sprayed material distributions.

Relationship between the Sprayed Material Distribution and Coating Time Figure 8 shows the representative temporal change in calculated mass distribution of the sprayed material. Each data were plotted on a normal probability graph. With an increase in coating time, mass distribution shifted to right. And finally, all particles passed through the coating zone, and there are no zero coated particles. Here, it is noteworthy that the simulated mass distribution of the sprayed material by our proposed model clearly showed a normal distribution function. This tendency has been also reported by Abe *et al.*,[16] who experimentally investigated mass distribution of the sprayed material in a tumbling fluidized bed coater, and Wnukowski and Setterwall,[5] who analyzed by analytical solution in a conventional fluidized bed. Therefore, validity of our proposed model based on the DEM–CFD coupling model was qualitatively confirmed.

Effect of Gas Velocity and Centrifugal Acceleration on Uniformity of Coated Particles Figure 9 shows the temporal change in the calculated and experimental variation coefficient of mass distribution of the sprayed material at different gas velocities. In both cases, centrifugal acceleration was set at 10 G at each condition. With an increase in coating time, calculated and experimental variation coefficients decreased at each gas velocity. This result implies that conditions of coated particles became more uniform with an increase in coating time. Additionally, with an increase in gas velocity, calculated variation coefficient decreased, because the particle mixing became more vigorous at higher gas velocity. These tendencies of calculated results qualitatively showed good agreement with the experimental results.

Figure 10 shows the relationship between calculated and experimental variation coefficient and coating time at different centrifugal accelerations. Here, gas velocities were set at 1.8 times of minimum fluidization velocity. With an increase in a centrifugal acceleration, calculated variation coefficient decreased. Figure 11 also indicates the average calculated circulation time of individual particle. The circulation time was defined as the period between going outside and entering coating zone. In this study, the average circulation time was calculated from temporal change of mass of the sprayed material within randomly selected 100 particles. The particle circulation time also decreased at a higher centrifugal acceleration due to higher rotational speed of vessel. Therefore, it was considered that mass distribution of the sprayed material became more uniform at higher centrifugal acceleration, because of smaller circulation time. In addition, numerical results also qualitatively showed good agreement with experimental ones (Fig. 10(2)).

In the present model, simulated results did not show quantitative agreement with experimental results due to the difference in the definition of coating. However, the effect of operating parameters on the uniformity (statistical indicator) of the coated particles could be qualitatively well simulated as mentioned previously. Therefore, these results indicate that

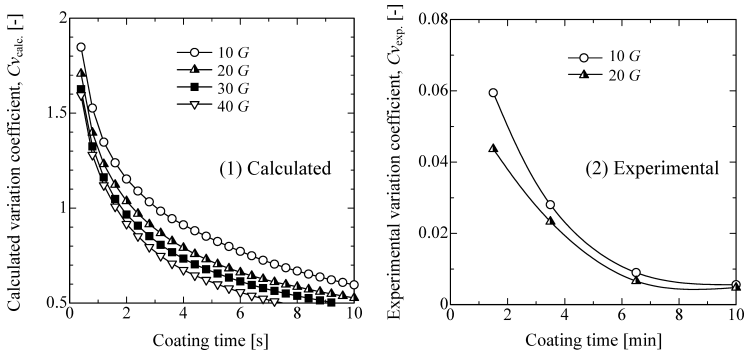

Fig. 10. Temporal Change in the Variation Coefficient of Mass Distribution at Different Centrifugal Accelerations

(1) and (2) show the calculated and experimental results, respectively. Gas velocity was set at 1.8 times of minimum fluidization velocity. Each solid line shows spline approximation curve.

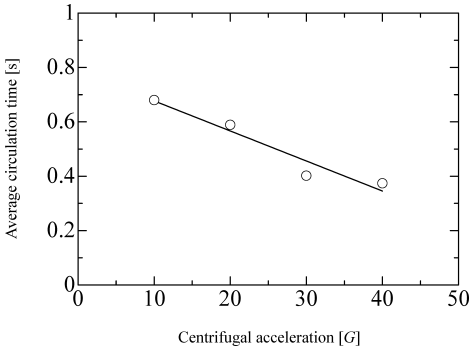

Fig. 11. Calculated Average Circulation Time at Different Centrifugal Accelerations

The solid line indicates least squares approximation line.

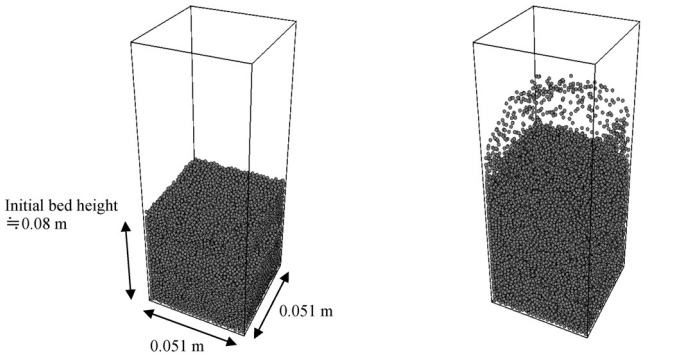

Fig. 12. Representative Snap Shots of Particle Configurations in a Conventional Fluidized Bed

our proposed simplified model could well analyze the fundamental mechanism of film coating process in a RFB.

Comparison of the Uniformity of Sprayed Material in a RFB with That in a Conventional Fluidized Bed In order to compare RFB coating process with conventional fluidized bed (FB) coating process, numerical simulation of film coating process in a conventional FB was also conducted. Figure 12 illustrates representative snapshots of initial condition and particle fluidization behavior in a FB. Here, calculation conditions in a FB were the same as that in a RFB, as shown in Table 2, except for coordinate system and fluid cell size. In the simulation of coating process, a spray nozzle was positioned at the top of the bed, and other simulation conditions of spray nozzle was also the same as that in a RFB.

Figure 13 shows temporal change in the calculated variation coefficient of mass distribution of the sprayed material in a FB and RFB (10 G). In both cases, gas velocity was set at 1.8 times of minimum fluidization velocity. From these results, variation coefficient in a RFB was much smaller than that in a conventional FB. Therefore, this result indicated that the uniformity of sprayed material on individual particle was improved in a RFB due to smaller circulation time. It was because the average circulation time of RFB (0.68 s) showed much smaller than that of FB (2.43 s), which is derived from rotating vessel, that is characteristic structure of RFB coater.

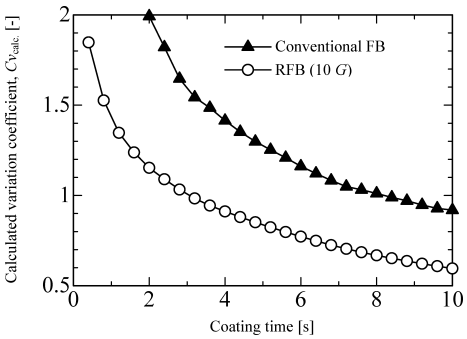

Fig. 13. Comparison of Calculated Variation Coefficient between a FB and RFB (u_0=1.8u_{mf})

Each solid line shows spline approximation curve.

Conclusions

In this study, numerical modeling and simulation of film coating process in a rotating fluidized bed was conducted. The calculated three-dimensional particle fluidization behavior in a RFB could be well simulated by using our proposed model, which is based on DEM–CFD coupling model. Distributions of the sprayed material could also be well visualized by our proposed model. Simulated sprayed material distributions could be expressed by a normal distribution function, which qualitatively showed the same results as experimental work by Abe *et al.*[16] and analytic solution by Wnukowski and Setterwall.[5] The calculated variation coefficient of mass distribution of the sprayed material decreased with an increase in a coating time, gas velocity and centrifugal acceleration. In addition, calculated results qualitatively showed good agreement with experimental results. From the

comparison of particle coating process in a RFB with that in a conventional FB by the numerical simulation, variation coefficient of mass distribution of the sprayed material in a RFB showed much smaller than that in a FB due to smaller circulation time. Therefore, it was indicated that the uniformity of sprayed material on individual particle was improved in a RFB.

Nomenclature

b	Colorfulness	[—]
C_D	Drug coefficient	[—]
C_m	Calculated mass of the sprayed material	[—]
Cv	Variation coefficient	[—]
d_p	Particle diameter	[m]
e	Restitution coefficient	[—]
$\boldsymbol{f}_i$	Volumetric particle–fluid interaction force	[N m^{-3}]
$\boldsymbol{F}_c$	Contact force	[N]
$\boldsymbol{F}_d$	Drag force	[N]
$\boldsymbol{F}_{cen}$	Centrifugal force	[N]
$\boldsymbol{F}_{cori}$	Coriolis force	[N]
$\boldsymbol{g}$	Gravity acceleration	[m s^{-2}]
G	Ratio of centrifugal acceleration to gravity acceleration on rotating vessel	[—]
k	Stiffness of spring	[N m^{-1}]
l	Moment of inertia of a particle	[kg m^{-2}]
m	Mass of a particle	[kg]
$\boldsymbol{n}$	Unit vector in the direction of normal contact	[—]
N	Number of particles	[—]
n_c	Number of particles in a fluid cell	[—]
n_s	Number of sample spots	[—]
P	Pressure	[Pa]
r	Radius for cylindrical coordinates	[m]
Re	Particle Reynolds number	[—]
t	Time	[s]
T_d	Specific vibration period in a mass-spring system	[s]
$\boldsymbol{u}$	Gas velocity	[m s^{-1}]
u_0	Superficial gas velocity	[m s^{-1}]
u_{mf}	Minimum fluidization velocity	[m s^{-1}]
$\boldsymbol{V}$	Particle velocity	[m s^{-1}]
$\boldsymbol{V}_r$	Relative particle velocity between contact particles	[m s^{-1}]
$\bar{\boldsymbol{V}}$	Average Particle velocity in a fluid cell	[m s^{-1}]
ΔV	Volume of a fluid cell	[m^3]
$\boldsymbol{X}$	Position vector of a particle	[m]
z	Depth for cylindrical coordinate	[m]

Greek letter

δ	Displacement between contact particles	[m]
ε	Voidage	[—]
η	Damping coefficient	[—]
μ	Friction coefficient	[—]
μ_f	Gas viscosity	[Pa s]
θ	Angular for cylindrical coordinates	[—]
ρ_f	Gas density	[kg m^{-3}]
ρ_p	Particle density	[kg m^{-3}]
σ	Standard deviation	[—]
ω_p	Angular velocity of a particle	[s^{-1}]

Subscript

r	Radius direction
θ	Angular direction
z	Depth direction
n	Normal direction
t	Tangential direction
exp.	Experimental
calc.	Calculated

References

1) Geldart D., *Powder Technol.*, **7**, 285—292 (1973).
2) Watano S., Imada Y., Hamada K., Wakamatu Y., Tanabe Y., Dave R. N., Pfeffer R., *Powder Techonol.*, **131**, 250—255 (2003).
3) Watano S., Nakamura H., Hamada K., Wakamatu Y., Tanabe Y., Dave R. N., Pfeffer R., *Powder Technol.*, **141**, 172—176 (2004).
4) Watano S., Nakamura H., Iwamoto D., Tanabe Y., Hamada K., *Powder Handling and Process.*, **15**, 390—394 (2003).
5) Wnukowski P., Setterwall F., *Chem. Eng. Sci.*, **44**, 493—505 (1989).
6) Nakamura H., Abe E., Yamada N., *Powder Technol.*, **99**, 140—146 (1998).
7) Tsuji Y., Kawaguchi T., Tanaka T., *Powder Technol.*, **77**, 79—87 (1993).
8) Anderson T. B., Jackson R., *I & EC Fundamentals*, **6**, 527—539 (1967).
9) Kuwagi K., Mikami T., Horio M., *Powder Technol.*, **109**, 27—40 (2000).
10) Ergun S., *Chem. Eng. Prog.*, **48**, 89—94 (1952).
11) Wen C. Y., Yu Y. H., *Chem. Eng. Prog. Symp. Ser.*, **62**, 100—111 (1966).
12) Patanker S. V., "Numerical Heat Transfer and Fluid Flow," Hemisphere, New York, 1980.
13) Cundall P. A., Strack O. D. L., *Geotechnique*, **29**, 47—65 (1979).
14) Mikami T., "Agglomerating Fluidization of Liquid/Solid Bridging Particles and Its Control," Doctor thesis of Tokyo University of Agriculture and Technology, 1998.
15) Qian G. H., Bagyi I., Burdick I. W., Pfeffer R., Shaw H., Steves J. G., *AIChE J.*, **47**, 1022—1034 (2001).
16) Abe E., Yamada N., Hirosue H., Nakamura H., *Powder Technol.*, **97**, 85—90 (1998).